Chinese Chemical Letters 33 (2022) 1385–1389

Contents lists available at ScienceDirect

Chinese Chemical Letters

journal homepage: www.elsevier.com/locate/cclet

Tuning band structure of graphitic carbon nitride for efficient degradation of sulfamethazine: Atmospheric condition and theoretical calculation

Yue Liu[a], Long Chen[b], Xiaona Liu[a], Tianwei Qian[a], Meng Yao[a], Wen Liu[b,c], Haodong Ji[b,c,*]

[a] College of Environmental Science and Engineering, Taiyuan University of Technology, Jinzhong 030600, China
[b] The Key Laboratory of Water and Sediment Science, Ministry of Education; College of Environment Science and Engineering, Peking University, Beijing 100871, China
[c] State Environmental Protection Key Laboratory of All Material Fluxes in River Ecosystems, Peking University, Beijing 100871, China

ARTICLE INFO

Article history:
Received 17 June 2021
Revised 12 July 2021
Accepted 9 August 2021
Available online 17 August 2021

Keywords:
Graphitic carbon nitride
Pharmaceuticals
Photocatalysis
Atmospheric condition
DFT calculation

ABSTRACT

Numerous approaches have been used to modify graphitic carbon nitride (g-C_3N_4) for improving its photocatalytic activity. In this study, we demonstrated a facial post-calcination method for modified graphitic carbon nitride (g-C_3N_4-Ar/Air) to direct tuning band structure, *i.e.*, bandgap and positions of conduction band (CB)/valence band (VB), through the control of atmospheric condition without involving any additional elements or metals or semiconductors. The synthesized g-C_3N_4-Ar/Air could efficiently degrade sulfamethazine (SMT) under simulated solar light, *i.e.*, 99.0% removal of SMT with rate constant $k_1 = 2.696\ h^{-1}$ within 1.5 h (4.9 times than pristine g-C_3N_4). Material characterizations indicated that the damaged/partial-collapsed structure and decreased nanosheet-interlayer distance for g-C_3N_4-Ar/Air resulted in the shift of band structure due to the denser stacking of pristine g-C_3N_4 through oxidative exfoliation and planarization by air calcination. In addition, the bandgap of g-C_3N_4-Ar/Air was slightly shrunk from 2.82 eV (pristine g-C_3N_4) to 2.79 eV, and the CB was significantly upshifted from −0.44 eV (pristine g-C_3N_4) to −0.81 eV, suggesting the powerful ability for donating the electrons for O_2 to form $^{\bullet}O_2^-$. Fukui index (f^-) based on theoretical calculation indicated that the sites of SMT molecule with high values, *i.e.*, N9, C4 and C6, preferred to be attacked by $^{\bullet}O_2^-$ and $^{\bullet}OH$, which is confirmed by the intermediates' analysis. The tuning method for graphitic carbon nitride provides a simple approach to regulate the charge carrier lifetime then facilitate the utilization efficiency of solar light, which exhibits great potential in efficient removal of emerging organic contaminants from wastewater.

© 2021 Published by Elsevier B.V. on behalf of Chinese Chemical Society and Institute of Materia Medica, Chinese Academy of Medical Sciences.

Since last decades, pharmaceuticals and personal care products (PPCPs) including antibiotics, antidepressants, anti-inflammatories, *etc.*, have been the emerging concerns in the environmental contaminants and drawn the researchers' focus due to the widely and frequently detection all around the world [1-6]. As the largest consumer and producer of PPCPs in the world, China has expended more than 2.5×10^7 kg antibiotics per year [7,8]. In addition, some researchers have investigated the detected PPCPs in Liaohe, Haihe, Yangtze, Pearl, Yellow, Songhuajiang Rivers watershed and the Liaodong Bay, Bohai Bay, Victoria Harbor *etc.* [1]. Among 65 antibiotics, three sulfonamides, *i.e.*, sulfamethazine (SMT), sulfamethoxazole (SMX) sulfadiazine (SD), are vastly detected throughout China [1,9]. Especially SMT was most detected in surface waters of China [1,10]. Although the detection concentration of SMT in water matrix is relatively low, it still shows high potential toxicity risks to ecosystem [2,11,12]. Furthermore, the conventional treatment technologies for drinking water, such as filtration, coagulation, and sedimentation, are not efficient to remove SMT [13]. In addition, some advanced oxidation technologies, *i.e.*, photocatalysis [2,14,15], electro-Fenton [16,17], and Fenton-like [18], have been used to degrade SMT in water. Therefore, treatment for wastewater containing PPCPs, especially improving the solar light response of photocatalysts, is urgent and prior demand.

Graphitic carbon nitride (g-C_3N_4) as a metal-free and two-dimensional layered structure, is an excellent catalyst with relative narrow bandgap of 2.7 eV and good visible light response [19,20], thus has drawn extensive concerns for environmental applications such as decontamination and disinfection [21]. In addition, some synthesis methods for g-C_3N_4 have been reported

* Corresponding author.
E-mail address: jihaodong@pku.edu.cn (H. Ji).

https://doi.org/10.1016/j.cclet.2021.08.061
1001-8417/© 2021 Published by Elsevier B.V. on behalf of Chinese Chemical Society and Institute of Materia Medica, Chinese Academy of Medical Sciences.

[19,22]. Moreover, the band structure of g-C_3N_4 can be tuned throughout the facial post-calcination method [22,23], which is not involving with foreign elements and other semiconductors. Some approaches, such as doping [24], heterostructure design [2,25], and surface modification [26,27], have been applied to improve the light absorption on visible light region and photocatalytic activity of catalysts. However, some defects caused by these foreign semiconductors or elements were ignored. In addition, for pristine g-C_3N_4, the direct tune of band structure can control the position of conduction band (CB) and valence band (VB) [22], which provides a simple approach to regulate the charge carrier lifetime and then facilitate the utilization efficiency of solar light.

Moreover, the photocatalytic degradation mechanisms of SMT were accurately and deeply evaluated by theoretical calculations, in specific Fukui index based on density functional theory (DFT). In recent years, our group has made lots of efforts on theoretical calculation, such as evaluation on reactive sites of organic pollutants [2,15,25,28-30], calculation on binding energy [31,32], transition state (TS) and potential energy surface (PES) [33,34], prediction on electrostatic potential [35].

In this work, the overall goal was to investigate the effects of polymerization atmosphere and synthesis condition for the photocatalytic activity of graphitic carbon nitride to degrade sulfamethazine. The detailed objectives were to: 1) Investigate the polymerization method to prepare the g-C_3N_4 under different atmosphere and conditions; 2) evaluate the photocatalytic degradation of SMT by various catalysts; 3) elucidate the mechanism of photocatalytic degradation of SMT and radical attacking *via* the combination method of the identification on degradation intermediates and analysis by theoretical chemistry; and 4) reveal the underlying mechanism of enhanced photocatalytic activity *via* material characterizations.

All chemicals were of analytical grade or higher in this work and described in Text S1 (Supporting information).

The photocatalysts based on graphitic carbon nitride (g-C_3N_4) derived from melamine were obtained by one-step modified polymerization method in accord with the literature [2,22]. In brief, 5 g of the melamine was directly put in a crucible, and heated in a tube furnace (Thermo Scientific, USA) to 550 °C at a rate of 15 °C/min under different calcination atmosphere and conditions (open or semi-closed), *i.e.*, static air atmosphere with semi-closed crucible for 3.5 h, air flow atmosphere with open crucible for 3.5 h, argon flow atmosphere with open crucible for 3.5 h, argon flow atmosphere with semi-closed crucible for 2 h following by air flow atmosphere for 1.5 h. Then the final photocatalysts were ground into powder and labeled as pristine g-C_3N_4, g-C_3N_4-open Air, g-C_3N_4-open Ar, and g-C_3N_4-Ar/Air.

Photocatalytic performances for various materials were investigated via sulfamethazine (SMT) degradation kinetic testes under simulated solar light. In the typical photocatalytic batch reaction, the initial SMT concentration (5 mg/L) and material dosage (0.2 g/L) were fixed in the quartz reactor (reaction volume 250 mL) with cooling system, then solution pH was adjusted to 7.0 ± 0.2 by diluted $HClO_4$ and NaOH (0.1 mol/L). After 2 h dark adsorption-desorption reaction (300 rpm), the photocatalytic reaction was initiated by turn-on the pre-heated light source, *i.e.*, simulated solar-light simulator system (PLS-SXE300D, Beijing Perfectlight Technology Co., Ltd.) with 300 W Xe lamp providing the 100 ± 0.5 mW/cm^2 light irradiation (AM 1.5G mode) as shown in Fig. S1 (Supporting information). At pre-determined intervals, the collected samples (each 1 mL) were straightway filtered *via* a nylon membrane (0.22 μm). Then the concentration of SMT and degradation intermediates in the filtrate was analyzed by high-performance liquid chromatography (HPLC) system (Agilent 1260 Infinity, USA) and ultra-high-performance liquid chromatography-mass spectroscopy system (UHPLC/MS/MS, Thermo scientific, USA),

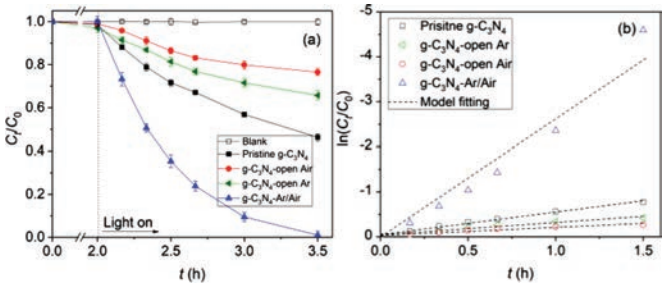

Fig. 1. Photocatalytic degradation of SMT by various catalysts synthesized by different calcination atmosphere and conditions (a) and linear fitting for corresponding kinetic data (b). Initial SMT = 5 mg/L, material dosage = 0.2 g/L, temperature = 25 ± 2 °C, initial pH: 7.0 ± 0.2, final pH: 7.0 ± 0.5.

respectively. The analytical details are described in the Text S2 (Supporting information). Control tests, *i.e.*, estimated degradation of SMT by simulated solar light (direct photolysis), were carried out without any catalysts but under otherwise identical conditions.

To identify the reactive oxygen species (ROS) during the photocatalytic reaction in this work, the generation of ROS was trapped using 5,5-dimethyl-1-pyrroline-*N*-oxide (DMPO) as spin-trapping agent, then observed the direct signals on a Bruker EMX/plus X-band (9.5 GHz) Electron Spin Resonance (ESR) spectrometer (Bruker, Billerica, MA) (details in Text S2).

The materials were characterized by transmission electron microscopy (TEM), X-ray diffraction (XRD), and X-ray photoelectron spectroscopy (XPS). Meanwhile, the band structures of the photocatalysts were analyzed by UV-visible absorption diffuse reflectance spectra (UV-vis DRS) and XPS-valence band (XPS-VB) (Text S3 in Supporting information).

To evaluate the reactive sites of SMT attacked by ROS, the theoretical calculation, *i.e.*, Fukui index derived from density functional theory (DFT) [15,25,29,30], was used to explain the insights of photocatalytic reaction on Gaussian 16 C.01 software [36] (details in Text S4 in Supporting information). Details on SMT optimized geometry and energy were given in Text S5 (Supporting information).

Fig. 1a presents the photocatalytic degradation of SMT by various catalysts synthesized by different calcination atmosphere and conditions, *i.e.*, pristine g-C_3N_4, g-C_3N_4-open Air, g-C_3N_4-open Ar, and g-C_3N_4-Ar/Air. Fig. 1b shows the linear fitting to SMT degradation in the photocatalytic system with various catalysts, and Table S1 (Supporting information) lists the fitted parameters. The pseudo-first order kinetic model is applied to interpret the kinetic data [37-40]:

$$\ln (C_t/C_0) = -k_1 t \quad (1)$$

where C_0 and C_t are the SMT concentrations (mg/L) at time 0 and t (h) in aqueous phase, respectively; and k_1 is the first-order rate constant (h^{-1}).

It is obvious that SMT is hard to be degraded by simulated solar light (< 0.1%) (Fig. 1a), *i.e.*, negligible direct photolysis. In addition, the adsorption of SMT by all catalysts was negligible (< 3%), which mainly can be attributed to the electrostatic repulsion between negative charged catalysts surface, for example, pH_{PZC} (g-C_3N_4) 5.1 [2] and the SMT species are the form of SMT^- and zwitterionic species of $SMT^{\pm}$ (Fig. S2 in Supporting information) at pH 7.0, and the lack of the π-π interaction, which is confirmed by other reports [2]. In addition, after light on, the SMT was significantly degraded in the presence of various catalysts, *i.e.*, 1.5 h SMT degradation reached 53.8% for pristine g-C_3N_4 (k_1 = 0.553 h^{-1}), 23.5% for g-C_3N_4-open Air (k_1 = 0.211 h^{-1}), 34.3% for g-C_3N_4-open Ar (k_1 = 0.320 h^{-1}), and 99.0% for g-C_3N_4-Ar/Air (k_1 = 2.696 h^{-1}). Compared to pristine g-C_3N_4, the photocatalytic activities of

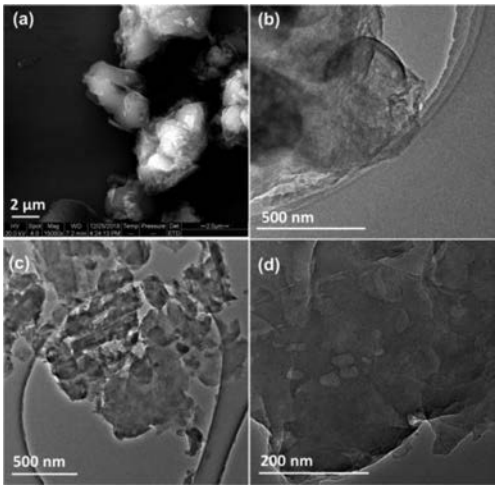

Fig. 2. SEM and TEM images of pristine g-C_3N_4 (a, b); TEM images of g-C_3N_4-Ar/Air (c, d).

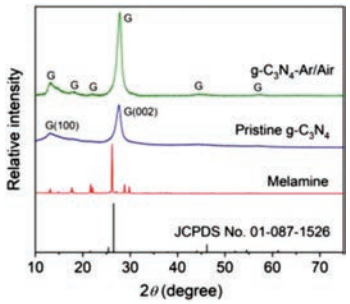

Fig. 3. XRD patterns of melamine, pristine g-C_3N_4, and g-C_3N_4-Ar/Air.

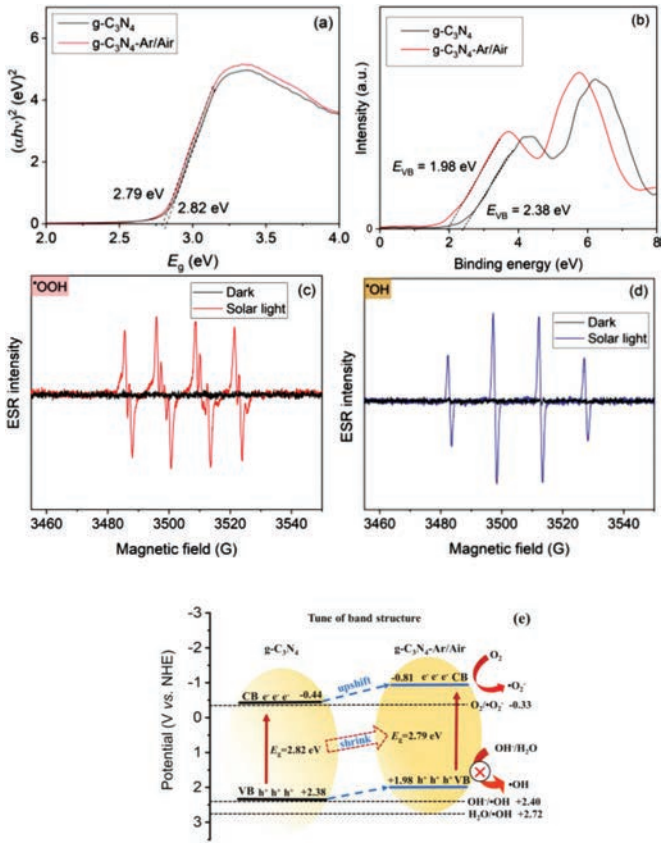

Fig. 4. Band gap (E_g) values calculated from Kubelka-Munk method (a) and XPS-VB (b) of various g-C_3N_4 catalysts; ESR spectra of DMPO-•OOH (c) and DMPO-•OH (d) in the presence of g-C_3N_4-Ar/Air under dark and solar light; tune of band structure on g-C_3N_4-Ar/Air (e).

g-C_3N_4-open Air and g-C_3N_4-open Ar were significantly retarded due to the partial formation of g-C_3N_4 and the existence of polymeric intermediates, *i.e.*, melam, melon, or melon sheet, resulted from the insufficient condensation/polymerization from melamine to g-C_3N_4 under open crucible condition [41]. However, the efficient degradation of SMT by g-C_3N_4-Ar/Air (99.0%, $k_1 = 2.696\ h^{-1}$, 4.9 times than pristine g-C_3N_4) was observed within 1.5 h, indicating the successful synthesis of g-C_3N_4-Ar/Air under argon atmosphere with semi-closed crucible for 2 h followed by air atmosphere for 1.5 h, which is consistent with other report [22].

Fig. 2 shows the SEM and TEM images of pristine g-C_3N_4, and TEM images of g-C_3N_4-Ar/Air. It is obvious that pristine g-C_3N_4, have a stacked-layer structure (Figs. 2a and b). However, the obtained g-C_3N_4-Ar/Air under Ar-Air-atmosphere exhibited the damaged and partial-collapsed structure (Figs. 2b and c), which is contributed by the release of gases, *i.e.*, NO, NO_2, NH_3, N_2/CO, CO_2 [22], during the polymerization/condensation of melamine, indicating the element loss of carbon and nitrogen. In addition, the released gases leading to hot bubbles (Fig. 2d), which is also observed and reported by other researchers [22,42,43], will result in the transformation from pristine g-C_3N_4 into g-C_3N_4-Ar/Air nanosheets *via* oxidative exfoliation process in the following air atmosphere (Figs. 2a-d) [22]. The morphology and structure variation caused by Ar/Air calcination led to the change of interlayer distance of melon sheets and the shift of band structure [22] which is further confirmed by the XRD results, then suggesting the visible-light absorption edge shift and possibly enhanced photocatalytic activity compared to pristine g-C_3N_4.

Fig. 3 presents XRD patterns of melamine, pristine g-C_3N_4, and g-C_3N_4-Ar/Air. All the distinctive peaks at 13.1°, 14.8°, 17.7°, 21.7°, 22.1°, 26.2°, 28.8° and 29.8° of melamine were disappeared and transferred to the two significant peaks in pristine g-C_3N_4, *i.e.*, 13.0° and 27.5° for the crystalline plane (100) and (002), respectively (JCPDS No. 01-087-1526) [2,25,26] *via* the static air calcination and polymerization. For g-C_3N_4-Ar/Air, two peaks assigned to (100) and (002) became sharper, indicating better crystalline phase. In addition, the peak of (002) in g-C_3N_4-Ar/Air was slightly shifted to 27.7° from original 27.5° in pristine g-C_3N_4, suggesting that the nanosheet-interlayer distance was decreased due to damaged/partial-collapsed structure and slightly denser stacking of pristine g-C_3N_4 through oxidative exfoliation and planarization by air calcination, which is consistent with previous TEM observations (Fig. 2d). Furthermore, the new peaks at 18.2°, 22.1°, 44.6°, and 57.2° appeared, indicating the layer-by-layer splitting and exfoliation of pristine g-C_3N_4. All above morphology, structure, and crystalline phase change resulted in the shift of band structure, therefore achieving the tune of band position, then improving the photocatalytic activity of g-C_3N_4 without any foreign elements or metals or semiconductors.

To further identify the bandgap and the position of band structure, *i.e.*, valence band (VB) and conduct band (CB) of g-C_3N_4-Ar/Air, diffuse reflectance UV-visible absorption spectra (UV-vis DRS) and X-ray photoelectron spectroscopy (XPS-VB) were analyzed respectively. In specific, the absorption spectra of different photocatalysts were directly obtained by UV-vis DRS, then the Kubelka-Munk transferred profiles (as shown in Fig. 4a) were calculated by following equation (Eq. 2) [2,25,44]:

$$\alpha h\nu = A(h\nu - E_g)^{n/2} \quad (2)$$

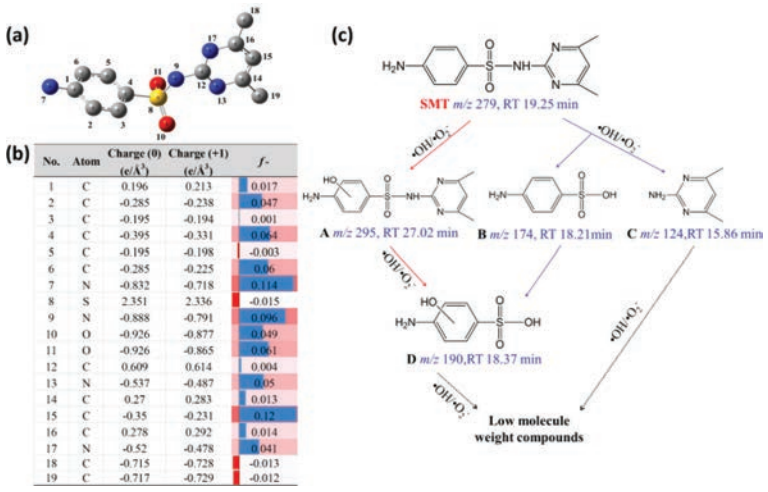

No.	Atom	Charge (0) (e/Å³)	Charge (+1) (e/Å³)	f⁻
1	C	0.196	0.213	0.017
2	C	-0.285	-0.238	0.047
3	C	-0.195	-0.194	0.001
4	C	-0.395	-0.331	0.064
5	C	-0.195	-0.198	-0.003
6	C	-0.285	-0.225	0.06
7	N	-0.832	-0.718	0.114
8	S	2.351	2.336	-0.015
9	N	-0.888	-0.791	0.096
10	O	-0.926	-0.877	0.049
11	O	-0.926	-0.865	0.061
12	C	0.609	0.614	0.004
13	N	-0.537	-0.487	0.05
14	C	0.27	0.283	0.013
15	C	-0.35	-0.231	0.12
16	C	0.278	0.292	0.014
17	N	-0.52	-0.478	0.041
18	C	-0.715	-0.728	-0.013
19	C	-0.717	-0.729	-0.012

Fig. 5. Chemical structure of SMT (a), natural population analysis (NPA) charges and Fukui index (f^-) of SMT (b) and degradation pathway of SMT in the photocatalysis system (c).

where α, h, ν, A, E_g are the absorption coefficient, Planck constant, photon frequency, constant, band gap energy, respectively. $n = 1$ for direct absorption and $n = 4$ for indirect absorption.

As shown in Fig. 4a, the band gap energy (E_g) of pristine g-C_3N_4 and g-C_3N_4-Ar/Air was 2.82 and 2.79 eV, indicating the slight red-shift and band shrinking for the modified g-C_3N_4 *via* the different calcination atmosphere, and resulting in the better photocatalytic activity, which is consistent with previous TEM and XRD observations. However, the E_g values of pristine g-C_3N_4 and g-C_3N_4-Ar/Air are close. Then the detailed band structures of photocatalysts were analyzed.

In addition, the VB of various catalysts was obtained by XPS-VB, and then the CB was calculated as below (Eq. 3):

$$E_{CB} = E_{VB} - E_g \tag{3}$$

According to Fig. 4b, the VB positions of pristine g-C_3N_4 and g-C_3N_4-Ar/Air were 2.38 and 1.98 eV, respectively, then the calculated CB positions of pristine g-C_3N_4 and g-C_3N_4-Ar/Air were −0.44 and −0.81 eV, respectively, indicating the band upshift in g-C_3N_4-Ar/Air, which is benefit to transfer electrons to O_2 forming $^{\bullet}O_2^-$. In addition, for g-C_3N_4-Ar/Air catalyst under solar light irradiation, the ESR spectra exhibited the existence of DMPO-$^{\bullet}$OOH (Fig. 4c) and DMPO-$^{\bullet}$OH (Fig. 4d) [22], indicating the generation of $^{\bullet}$OOH, which is derived from the protonation process of superoxide radical ($^{\bullet}O_2^-$), and $^{\bullet}$OH. Therefore, the dominant mechanism for SMT degradation by g-C_3N_4-Ar/Air under simulated solar light in this work is radical attacking by $^{\bullet}O_2^-$ and $^{\bullet}$OH. The details on the generation mechanism of radicals and the degradation pathway of SMT in the photocatalytic system will be demonstrated in the following section based on intermediates analysis and theoretical calculation.

Fig. 4e elucidates the enhanced mechanism on photocatalytic activity of g-C_3N_4-Ar/Air. Based on the the Kubelka-Munk transferred profiles (Fig. 4a derived from UV-vis DRS) and XPS-VB (Fig. 4b), the VB positions of pristine g-C_3N_4 (2.38 eV) and g-C_3N_4-Ar/Air (1.98 eV), *i.e.* h_{VB}^+ in both catalysts, were hard to oxidize the H_2O or OH^- to generate $^{\bullet}$OH due to less redox potential than H_2O or $OH^-/^{\bullet}OH$ (2.72 or 2.40 V *vs.* NHE), respectively [2,45,46]. Moreover, the CB position in g-C_3N_4-Ar/Air was upshifted from −0.44 eV of pristine g-C_3N_4 to −0.81 eV, suggesting the powerful ability on donating the electrons for O_2 to form $^{\bullet}O_2^-$ ($O_2/^{\bullet}O_2^- = -0.33$ V vs. NHE) [46,47]. In addition, the detection of DMPO-$^{\bullet}$OOH, which is due to the protonation of $^{\bullet}O_2^-$ in the aqueous phase, also strongly supported the aforementioned results. However, $^{\bullet}$OH was also detected although h_{VB}^+ in g-C_3N_4-Ar/Air cannot directly oxidize the H_2O or OH^-, which is mainly attributed by the radical chain reactions and transferred from $^{\bullet}O_2^-$ [48-52]. Then for g-C_3N_4-Ar/Air, the combination of narrower E_g and more negative CB is benefited and favored to generate highly active CB-e^-, resulting in the enhnanced photocatalytic activity than pristine g-C_3N_4. The dominant mechanism on the generation of radicals in this photocatalytic system can be summarized as follows:

$$\text{g-}C_3N_4\text{-Ar/Air} + h\nu \rightarrow \text{g-}C_3N_4\text{-Ar/Air}\ (e^- - h^+) \tag{4}$$

$$O_2 + \text{CB-}e^- \rightarrow {}^{\bullet}O_2^- \tag{5}$$

$${}^{\bullet}O_2^- + 2e^- + 2H^+ \rightarrow {}^{\bullet}OH + OH^- \tag{6}$$

$$\text{SMT} + {}^{\bullet}O_2^-/{}^{\bullet}OH \rightarrow \text{intermediates} \rightarrow \text{products} + CO_2 \tag{7}$$

$$\text{SMT} + h^+ \rightarrow \text{intermediates} \rightarrow \text{products} + CO_2 \tag{8}$$

Based on DFT, the optimized geometry structure of SMT was presented in Fig. 5a and the optimized cartesian coordinates were listed in Text S5 (Supporting information). Then the Fukui index, f^- in this study, was used to predict the reactive sites on SMT molecule by electrophilic attack, which was shown in Fig. 5b. Furthermore, superoxide ($^{\bullet}O_2^-$) and hydroxyl ($^{\bullet}$OH) radicals are the primary reactive oxygen species (ROS) in this photocatalytic degradation system. Both of these two radicals preferred to attack the electron-rich sites of SMT, thus categorized as electrophilic radicals [2,28,34,53]. In addition, the identified photocatalytic degradation intermediates (IMs) of SMT in this system are presented in Fig. 5c. High f^- value on SMT molecule suggested that the sites preferred to lose electron then be attacked by $^{\bullet}O_2^-$ and $^{\bullet}$OH. In specific, the C15 ($f^- = 0.12$), N7 ($f^- = 0.114$), and N9 ($f^- = 0.096$) are ranked in the first-stage reactive sites of SMT. Then the following stages are the reactive site on benzene ring, *i.e.*, C4 ($f^- = 0.064$) and C6 ($f^- = 0.06$). Considering the detailed reaction conditions, *i.e.*, at neutral pH, the N–S bond cleavage will occur due to radical attacking on the high f^- value of N9 in the first-stage reactive site of SMT, resulting in the formed IMs of B and C, which is confirmed by UHPLC/MS/MS detection (Fig. 5c). Meanwhile, the IM **A** was generated due to $^{\bullet}$OH addition, which is consistent with the prediction of benzene ring in the second-stage. Then, IM **D** was formed throughout the further radical attacking on IMs **A** or **B**.

After further deep oxidation by ROS, low molecular weight compounds were produced then transformed into the final mineralization products (CO_2 and H_2O).

In conclusion, we demonstrated the tuning process of band structure for graphitic carbon nitride through the control of atmospheric condition without involving any foreign elements or metals or semiconductors, which can efficiently photocatalytic degrade SMT under simulated solar light, *i.e.*, 99.0% removal of SMT by g-C_3N_4-Ar/Air with rate constant $k_1 = 2.696\ h^{-1}$ within 1.5 h (4.9 times than pristine g-C_3N_4). TEM and XRD confirmed the damaged/partial-collapsed structure and decreased nanosheet-interlayer distance due to the denser stacking of pristine g-C_3N_4 through oxidative exfoliation and planarization by air calcination. Then the change of morphology and structure will result in the shift of band structure, *i.e.*, the bandgap of g-C_3N_4-Ar/Air was shrunk from 2.82 eV (pristine g-C_3N_4) to 2.79 eV, and the CB was upshifted from −0.44 eV (pristine g-C_3N_4) to −0.81 eV, indicating the higher potential power for transferring electrons to oxygen, then achieving the tune of band position and improving the photocatalytic activity. Fukui index (f^-) based on DFT calculation indicated that the sites of SMT molecule with high value, *i.e.*, N9, C4 and C6, preferred to be attacked by the produced electrophilic radicals ($^{\bullet}O_2^-$ and $^{\bullet}OH$), resulting in the N–S bond cleavage and hydroxyl radical addition. In addition, the prediction of reactive sites on SMT is confirmed by the formation of intermediates *via* UHPLC/MS/MS analysis. The tuning method for graphitic carbon nitride is a promising procedure for photocatalyst modification, which exhibits great potential in efficient removal of emerging organic contaminants from wastewater.

Declaration of competing interest

The authors declare that they have no known competing financial interests or personal relationships that could have appeared to influence the work reported in this paper.

Acknowledgments

This work was partially supported by the National Natural Science Foundation of China (Nos. 21906001, 52100069, 51721006 and 41272375), Beijing Nova Program (No. Z191100001119054), the Fundamental Research Funds for the Central Universities (No. BFUKF202118), and China Postdoctoral Science Foundation (No. 2021M690208).

Supplementary materials

Supplementary material associated with this article can be found, in the online version, at doi:10.1016/j.cclet.2021.08.061.

References

[1] Q. Bu, B. Wang, J. Huang, et al., J. Hazard. Mater. 262 (2013) 189–211.
[2] H. Ji, P. Du, D. Zhao, et al., Appl. Catal. B: Environ. 263 (2020) 118357.
[3] J.L. Liu, M.H. Wong, Environ. Int. 59 (2013) 208–224.
[4] J. Wang, S. Wang, J. Environ. Manage. 182 (2016) 620–640.
[5] J.B. Ellis, Environ. Pollut. 144 (2006) 184–189.
[6] J. Xu, J. Chen, Y. Ao, et al., Chin. Chem. Lett. 32 (2021) 3226–3230.
[7] W.H. Xu, G. Zhang, S.C. Zou, et al., Environ. Pollut. 145 (2007) 672–679.
[8] B.J. Richardson, P.K.S. Lam, M. Martin, Mar. Pollut. Bull. 50 (2005) 913–920.
[9] S. Yanan, X. Xing, Q. Yue, et al., Environ. Sci. Nano 7 (2020) 1444–1453.
[10] K. Kümmerer, Chemosphere 75 (2009) 417–434.
[11] J. Tang, J. Wang, Environ. Sci. Technol. 52 (2018) 5367–5377.
[12] X. Liu, F. Huang, Y. Yu, et al., Chemosphere 226 (2019) 103–109.
[13] C. Aristizabal-Ciro, A.M. Botero-Coy, F.J. López, et al., Environ. Sci. Pollut. Res. 24 (2017) 7335–7347.
[14] Y. Song, J. Tian, S. Gao, et al., Appl. Catal. B: Environ. 210 (2017) 88–96.
[15] X. Liu, H. Ji, S. Li, et al., Chemosphere 233 (2019) 198–206.
[16] F. Sopaj, N. Oturan, J. Pinson, et al., Appl. Catal. B: Environ. 199 (2016) 331–341.
[17] J. Li, Y. Li, Z. Xiong, et al., Chin. Chem. Lett. 30 (2019) 2139–2146.
[18] T. Zhou, X. Wu, Y. Zhang, et al., Appl. Catal. B: Environ. 136-137 (2013) 294–301.
[19] X. Wang, S. Blechert, M. Antonietti, ACS Catal. 2 (2012) 1596–1606.
[20] Z. Zhao, Y. Sun, F. Dong, Nanoscale 7 (2015) 15–37.
[21] W.J. Ong, L.L. Tan, Y.H. Ng, et al., Chem. Rev. 116 (2016) 7159–7329.
[22] J. Xiao, Q. Han, H. Cao, et al., ACS Catal. 9 (2019) 8852–8861.
[23] Y. Wang, X. Wang, M. Antonietti, Angew. Chem. Int. Ed. 51 (2012) 68–89.
[24] H. Wang, J. Zhang, P. Wang, et al., Chin. Chem. Lett. 31 (2020) 2789–2794.
[25] D. Zhang, J. Qi, H. Ji, et al., Chem. Eng. J. 400 (2020) 125918.
[26] W. Liu, Y. Li, F. Liu, et al., Water Res. 151 (2019) 8–19.
[27] Y. Xing, X. Wang, S. Hao, et al., Chin. Chem. Lett. 32 (2021) 13–20.
[28] M. Ma, L. Chen, J. Zhao, et al., Chin. Chem. Lett. 30 (2019) 2191–2195.
[29] F. Pan, H. Ji, P. Du, et al., J. Hazard. Mater. 402 (2021) 123779.
[30] L. Chen, H. Ji, J. Qi, et al., Chem. Eng. J. 406 (2021) 126877.
[31] W. Sun, H. Li, H. Li, et al., Chem. Eng. J. 360 (2019) 645–653.
[32] T. Xu, H. Ji, Y. Gu, et al., Chem. Eng. J. 388 (2020) 124230.
[33] S. Li, T. Huang, P. Du, et al., Water Res. 185 (2020) 116286.
[34] H. Ji, W. Liu, F. Sun, et al., Chem. Eng. J. 419 (2021) 129605.
[35] H. Ji, T. Wang, T. Huang, et al., J. Cleaner Prod. 278 (2021) 123924.
[36] M.J. Frisch, G.W. Trucks, H.B. Schlegel, et al., Gaussian 16 Rev. C.01, Wallingford, CT, 2016.
[37] M.J. Alowitz, M.M. Scherer, Environ. Sci. Technol. 36 (2002) 299–306.
[38] Q. Chen, L. Chen, J. Qi, et al., Chin. Chem. Lett. (2019) 1214–1218.
[39] H. Ji, Y. Zhu, J. Duan, et al., Chin. Chem. Lett. 30 (2019) 2163–2168.
[40] W. Liu, W. Zhang, M. Liu, et al., Chin. Chem. Lett. 30 (2019) 2177–2180.
[41] A. Thomas, A. Fischer, F. Goettmann, et al., J. Mater. Chem. 18 (2008) 4893–4908.
[42] J. Xiao, J. Rabeah, J. Yang, et al., ACS Catal. 7 (2017) 6198–6206.
[43] P. Niu, L. Zhang, G. Liu, H.M. Cheng, Adv. Funct. Mater. 22 (2012) 4763–4770.
[44] C. Feng, F. Teng, Z. Liu, et al., J. Mol. Catal. A: Chem. 401 (2015) 35–40.
[45] J. Aliaga, N. Cifuentes, G. González, et al., Catalysts 8 (2018) 374.
[46] T. Lv, D. Li, Y. Hong, et al., Dalton Trans. 46 (2017) 12675–12682.
[47] M. Reli, P. Huo, M. Šihor, et al., J. Phys. Chem. A 120 (2016) 8564–8573.
[48] Y. Jin, Y. Shi, Z. Chen, et al., Appl. Catal. B: Environ. 267 (2020) 118730.
[49] Y. Jin, Y. Shi, R. Chen, et al., Chemosphere 215 (2019) 380–387.
[50] Z. Xiong, B. Lai, P. Yang, Water Res. 140 (2018) 12–23.
[51] Z. Xiong, B. Lai, Y. Yuan, et al., Chem. Eng. J. 302 (2016) 137–145.
[52] X. Wang, X. Pu, Y. Yuan, et al., Chin. Chem. Lett. 31 (2020) 2634–2640.
[53] F. De Vleeschouwer, V. Van Speybroeck, M. Waroquier, et al., Org. Lett. 9 (2007) 2721–2724.